

Massive Clusters in the Inner Regions of NGC 1365: Cluster Formation and Gas Dynamics in Galactic Bars

Bruce G. Elmegreen

IBM Research Division, T.J. Watson Research Center, 1101 Kitchawan Road, Yorktown Heights, NY 10598, USA

bge@watson.ibm.com

Emmanuel Galliano

Observatorio Nacional, Rua General José Cristino, 77, 20921-400, São Cristovão, Rio de Janeiro, Brazil

egallian@on.br

Danielle Alloin

Laboratoire AIM, CEA/DSM-CNRS-Université Paris Diderot, IRFU/Service d'Astrophysique, Bât.709, CEA/Saclay, F-91191 Gif-sur-Yvette Cedex, France

danielle.alloin@cea.fr

ABSTRACT

Cluster formation and gas dynamics in the central regions of barred galaxies are not well understood. This paper reviews the environment of three $10^7 M_{\odot}$ clusters near the inner Lindblad resonance of the barred spiral NGC 1365. The morphology, mass, and flow of HI and CO gas in the spiral and barred regions are examined for evidence of the location and mechanism of cluster formation. The accretion rate is compared with the star formation rate to infer the lifetime of the starburst. The gas appears to move from inside corotation in the spiral region to looping filaments in the interbar region at a rate of $\sim 6 M_{\odot} \text{ yr}^{-1}$ before impacting the bar dustlane somewhere along its length. The gas in this dustlane moves inward, growing in flux as a result of the accretion to $\sim 40 M_{\odot} \text{ yr}^{-1}$ near the ILR. This inner rate exceeds the current nuclear star formation rate by a factor of 4, suggesting continued buildup of nuclear mass for another ~ 0.5 Gyr. The bar may be only 1-2 Gyr old. Extrapolating the bar flow back in time, we infer that the clusters formed in the bar dustlane outside the central dust ring at a position where an interbar filament currently impacts the lane. The ram pressure from this impact is comparable to the pressure in the bar dustlane, and both are comparable to the pressure in the massive clusters. Impact triggering is suggested. The isothermal assumption in numerical simulations seems inappropriate for the rarefaction parts of spiral and bar

gas flows. The clusters have enough lower-mass counterparts to suggest they are part of a normal power law mass distribution. Gas trapping in the most massive clusters could explain their [NeII] emission, which is not evident from the lower-mass clusters nearby.

Subject headings: stars: formation — galaxies: individual (NGC 1365) — galaxies: spiral — galaxies: star clusters — galaxies: starburst

1. Introduction

Massive clusters in the inner regions of barred spiral galaxies are often observed as “hotspots” in the Lindblad resonance ring (Morgan 1958; Sersic & Pastoriza 1965). They have been studied using visible, ultraviolet, near-infrared and radio wavelengths (e.g. Hummel et al. 1987; Benedict et al. 1993; Barth et al. 1995; Meurer et al. 1995; Tacconi-Garman et al. 1996; Maoz et al. 1996; Böker et al. 2008). In a recent study using near-infrared (NIR) and mid-infrared (MIR) images and spectra, Galliano et al. (2005, 2008; hereafter G08) found three compact clusters with masses of around $10^7 M_{\odot}$ in the ILR ring region of NGC 1365 (see also Kristen et al. 1997). These clusters are somewhat equally spaced in a dense dusty region where their extinction and MIR continuum emission suggest they are still embedded. Their ages are between 6 and 8 Myr.

This paper reviews the environment of the three clusters in an attempt to understand how they formed. We consider the cluster ages and masses from G08, the distribution of gas mass and velocity from HI observations by Jörsäter & van Moorsel (1995; hereafter JM95) and CO observations by Sakamoto et al. (2007; hereafter S07), the likely gas flow in the bar using models of NGC 1365 by Lindblad, Lindblad & Athanassoula (1996, hereafter L96), and the total accretion rate in comparison to the star formation rate. These observations, along with a detailed optical image of dust filaments in the galaxy, suggest that the gas inside corotation spirals into the interbar region and hits the bar dustlane after half of a rotation relative to the pattern. There it shocks against the gas already in the bar dustlane, and both fall directly to the central region. The result is a high pressure at various places along the dustlane that can drive massive cluster formation, and a high gas accretion rate to the center that can sustain the observed starburst for several hundred Myr.

The flow of gas to the inner regions of barred galaxies is well observed (e.g. Ishizuki et al. 1990; Regan, Vogel & Teuben 1997; Regan, Sheth, & Vogel 1999; Knapen et al. 2000), as is the accumulation of gas after this inflow has occurred (e.g., Kenney et al. 1992; Sakamoto et al. 1999; Sheth et al. 2005; Jogee et al. 2005). The gas often makes a ring near the ILR (e.g., Regan et al. 2002) as a result of gas shocking where the stable orbits change from aligned with the bar to perpendicular (Sanders & Huntley 1976; Combes & Gerin 1985; Regan & Teuben 2003). Star formation in or near this ILR ring is common (see review in Buta & Combes 1996; Kormendy & Kennicutt 2004). There have been several models for this star formation, including gravitational instabilities in the ILR ring (Elmegreen 1994), gravitational instabilities in dense spurs preceding

the straight dust lane (Sheth et al. 2000, 2002; Asif et al. 2005; Zurita & Pérez 2008), and gas impact triggering where the ring meets the straight bar dust lane (Böker et al. 2008; Meier, Turner, & Hurt 2008). Aspects of all three models are evident in the present observations. Zurita et al. (2004) noticed, in addition, an enhancement in star formation at minima of the velocity gradient along the bar dust lane in NGC 1530; they suggested that local shocks and compressions at these gradient minima trigger star formation.

We also consider the unusually large cluster masses and question whether they are part of a power law mass function, as typically found in galaxy disks, or a characteristic mass in some physical process that produces a peaked mass function. The difference in mass functions is important for old globular clusters, which have been claimed in various studies to have evolved from either one or the other of these two functions (e.g., compare Vesperini 2000, Fall & Zhang 2002, Parmentier & Gilmore 2005). We see tentative evidence for lower-mass clusters in the dustlane, suggesting there is an underlying power law in the cluster mass function. Maoz et al. (2001) found M^{-2} power law mass functions for ILR ring clusters in two other galaxies.

In what follows, section 2 provides a summary of the physical parameters of the three cluster environments, while in section 3, we discuss their likely formation site. In sections 4 and 5, we examine the gas accretion, star formation rates, and implications for the bar age. Information about the cluster mass function is examined in section 6. The removal of gas from massive clusters is discussed in section 7, and a possible mechanism for their formation is in section 8. The conclusions are in section 9.

2. Characteristics and environment of the three ILR clusters in NGC 1365

The three massive clusters in NGC 1365, designated M4, M5, and M6, were discovered in the MIR by Galliano et al. (2005) and studied in more detail by G08. They were also observed as radio continuum sources by Sandqvist et al. (1995), Forbes & Norris (1998), and Morganti et al. (1999), and detected in CO(2-1) by S07. In what follows, we review the properties of the three clusters given by G08 using a distance to NGC 1365 of 18.6 Mpc. The CO properties are summarized from S07, with values converted from the distance they assume, 17.95 Mpc, to 18.6 Mpc.

Figure 1 shows an image of NGC 1365 from ESO. It is a combination from three exposures with FORS1: B(blue), V(green), and R(Red) ¹ with illustrations of various topics discussed in this paper. The three clusters are associated with dust structures at the position where the north-eastern bar dustlane enters the ILR dust ring. Cluster M5 is at the edge of the dustlane and more prominent optically. This is consistent with extinctions from the $\text{Br}\gamma/\text{Br}\alpha$ ratio, which equal $A_V = 13.5, 3.2,$ and 8.5 mag., respectively for M4, M5, and M6 (G08). Bright nebular emission from $\text{P}\alpha$, $\text{Br}\gamma$, $\text{Br}\alpha$, and $[\text{NeII}]$ suggest local ionization of the dustlane by the clusters; $2\mu\text{m}$ H_2

¹<http://www.eso.org/public/outreach/press-rel/pr-1999/phot-08-99.html>

lines indicate local heating of molecules. Local ionization is also suggested by an unusually strong $8.6\mu\text{m}$ feature that is presumably from ionized PAHs. Thus the clusters are most likely embedded in dust and associated with dense gas (G08).

There is an unusual lack of [ArIII] and [SIV] emission from all three clusters which indicates that the radiation field is weak in the far-ultraviolet (G08). This implies that the most massive remaining stars are only $20 - 25 M_{\odot}$, and therefore suggests a time larger than 6 Myr from the last event of significant star formation. The presence of non-thermal centimeter emission and $2.3\mu\text{m}$ CO absorption bands also constrains the age to be greater than several Myr. An upper limit to the cluster ages is ~ 8 Myr from the requirement that the total mass in all three clusters be significantly less than the gas mass in the inner kpc of the galaxy. For an age of 7 Myr, the cluster masses are on the order of $10^7 M_{\odot}$.

The ILR region of NGC 1365 was mapped at $2''$ resolution in three isotopes of CO(2-1) by S07. They assumed a conversion of ^{12}CO to H_2 equal to $X_{\text{CO}} = 0.5 \times 10^{20} \text{ cm}^{-2} (\text{km s}^{-1})^{-1}$, which is comparable to that estimated for the center of the Milky Way but smaller than the usual value applied to galactic disks. High temperature CO would make X_{CO} small like this. They checked X_{CO} by comparing the ^{12}CO (2-1) mass to the C^{18}O (2-1) mass and got the reasonable result that the latter was smaller by a factor of ~ 2 , which is to be expected for the denser C^{18}O (2-1) regions compared to the total. We assume the same conversion factor here. A similar low CO conversion factor was proposed by Meier, Turner, & Hurt (2008) for nuclear emission in Maffei 2.

The total CO mass in the inner one kpc radius was determined by S07 to be $9 \times 10^8 M_{\odot}$, which converts to $9.7 \times 10^8 M_{\odot}$ at the higher distance. (In what follows, we keep additional significant figures like this in evaluations from other studies, even though the observations and conversion factors may not warrant this much accuracy, to keep track of the various distance conventions. The final results are rounded off in summary statements.) The average column density is $290 M_{\odot} \text{ pc}^{-2}$. The region enclosing clusters M4, M5, and M6 has a higher mean column density, $\sim 500 M_{\odot} \text{ pc}^{-2}$, peaking at around $800 M_{\odot} \text{ pc}^{-2}$. Cluster M4 has a distinct molecular cloud associated with it (S07), with a distance-converted mass of $5.4 \times 10^7 M_{\odot}$ and a peak column density at the limit of resolution of $\sim 900 M_{\odot} \text{ pc}^{-2}$. This cloud mass is ~ 5.4 times the mass of the cluster so the efficiency of star formation was $\sim 1/6.4 = 16\%$. Clusters M5 and M6 also have associated CO peaks (S07), although they are not as prominent as the one around M4.

The CO mass in the entire bar was estimated by Sandqvist et al. (1995) to be $20 \times 10^9 M_{\odot}$ using $X_{\text{CO}} = 2.3 \times 10^{20} \text{ cm}^{-2} (\text{km s}^{-1})^{-1}$. They assumed a distance of 20 Mpc. With our distance of 18.6 Mpc, the bar CO mass becomes $17 \times 10^9 M_{\odot}$, and with the Sakamoto et al. (2007) value of X_{CO} , the bar CO mass is $3.8 \times 10^9 M_{\odot}$. According to the previous paragraph, $0.97 \times 10^9 M_{\odot}$, or 26% of the total bar CO is currently in the central 1 kpc radius. There is little HI emission in the bar region (Sandqvist et al 1995), so this total is what is available for ILR star formation after it accretes to the center.

The velocity dispersion of the gas that formed the clusters can be estimated from the cluster

virial speed, because a cluster forms in the potential well of its local cloud core. For a cluster mass of $10^7 M_\odot$ and a radius of 5 pc (G08), the virial speed in a uniform sphere is $\sim 40 \text{ km s}^{-1}$. The velocity dispersion of the gas can also be measured directly. The FWHM of the CO line around cluster M4 is 70 km s^{-1} (S07, Table 5), so the Gaussian dispersion is 30 km s^{-1} , similar to the likely cluster dispersion. The CO gas regions around M5 and M6 have similar dispersions (S07). The CO velocity dispersion in the bar dustlane may be obtained from the position-velocity diagram in Figure 6 of S07, and it is about the same, 30 km s^{-1} . We therefore assume the gas velocity dispersion is $\sim 30 \text{ km s}^{-1}$. This is high compared to observed dispersions in the outer parts of disk galaxies. In the inner regions of NGC 1365 there is a deep potential well and a lot of energy available for gas agitation in the motion of the bar and in the relative motions of gas streams.

A velocity dispersion of $\sigma = 30 \text{ km s}^{-1}$ makes the cloud around M4 close to virialized: the virial mass inside the telescope beam with radius $R = 115 \text{ pc}$ is $M_V \sim 5R\sigma^2/G = 1.2 \times 10^8 M_\odot$, which is a factor of only 2.2 higher than the CO-derived H_2 mass. We can also set an upper limit to the CO cloud size using the extent of the source in the narrow filter [NeII] $12.8 \mu\text{m}$ image (G08). In this image, the FWHM of the source is $\sim 0.5''$. If we identify this FWHM with the cloud diameter, then the radius would be 45 pc and the virial mass $5.1 \times 10^7 M_\odot$, which is about the same as the CO mass.

The column densities can now be used to determine the gaseous scale height. S07 estimated from the CO rotation curve that the stellar mass inside the inner 1 kpc radius is $10^{10} M_\odot$, so the average stellar mass column density is $3200 M_\odot \text{ pc}^{-2}$. The molecular gas layer is probably thinner than the stellar layer, so stellar gravity adds to gas gravity in establishing the gas layer thickness. For a two-fluid disk, the midplane gas pressure is approximately (Elmegreen 1989)

$$P = (\pi/2) G \Sigma_{gas} \left(\Sigma_{gas} + \frac{\sigma_{gas}}{\sigma_{stars}} \Sigma_{stars} \right) \quad (1)$$

and the midplane gas density is $\rho_{gas,0} = P/\sigma_{gas}^2$. Here, Σ is the mass column density of either gas or stars, and σ is the velocity dispersion; G is the gravitational constant. The scale height is $H_{gas} = \Sigma_{gas} / (2\rho_{gas,0})$, which is

$$H_{gas} \approx \frac{\sigma_{gas}^2}{\pi G (\Sigma_{gas} + [\sigma_{gas}/\sigma_{stars}] \Sigma_{stars})}. \quad (2)$$

Setting $\Sigma_{gas} = 290 M_\odot$ for the average value in the inner kpc, $\Sigma_{stars} = 3200 M_\odot \text{ pc}^{-2}$, $\sigma_{gas} = 30 \text{ km s}^{-1}$, and $\sigma_{stars} = 100 \text{ km s}^{-1}$ from Emsellem et al. (2001), the gas scale height becomes $230 / (1 + 3.3) \sim 50 \text{ pc}$. It follows that the average midplane gas density is $\rho_{gas,0} = 2.9 M_\odot \text{ pc}^{-3}$, which corresponds to an average H_2 density of 50 cm^{-3} in the inner kpc. The corresponding pressure would be this density multiplied by σ^2 , or $1.3 \times 10^7 k_B$ for Boltzmann's constant k_B . The stellar column density dominates the gas in this evaluation of scale height, so in the dense region surrounding the three clusters, where the average H_2 column density is $\sim 500 M_\odot \text{ pc}^{-2}$, the scale height is about the same, $\sim 45 \text{ pc}$, although the average density is higher, $5.5 M_\odot \text{ pc}^{-3}$, or $95 \text{ H}_2 \text{ cm}^{-3}$. The stellar scale height is $H_{stars} = \sigma_{stars}^2 / (\pi G [\Sigma_{gas} + \Sigma_{stars}]) \sim 210 \text{ pc}$.

In summary, three $\sim 10^7 M_\odot$ clusters, ~ 7 Myr old, are each projected against molecular clouds in the ILR region of NGC 1365. The clouds have masses of several $\times 10^7 M_\odot$ and column densities of $500 - 900 M_\odot \text{ pc}^{-2}$. They are part of a dense massive dustlane in the northeast that connects the ILR region to the outer part of the bar. A similar dustlane is in the south west part of the bar. The total molecular mass in the bar is $\sim 3.8 \times 10^9 M_\odot$, of which $\sim 26\%$ is in the inner kpc region near the ILR. The velocity dispersion in the molecular gas is $\sim 30 \text{ km s}^{-1}$, which suggests the individual clouds are virialized, the average gas pressure in the inner kpc is $\sim 10^7 k_B$, the gas scale height is $\sim 50 \text{ pc}$, and the average gas density is $\sim 50 \text{ H}_2 \text{ molecules cm}^{-3}$. In the CO plateau around the 3 clusters, the average H_2 density is $\sim 95 \text{ cm}^{-3}$.

3. Where the clusters formed

The birthplace of the clusters can be assessed from the CO velocities, the cluster ages, and the bar pattern speed. The clusters have projected distances from the galactic center of 640 pc, 920 pc, and 760 pc (G08), respectively, which correspond to 800 pc to 900 pc in the deprojected frame. According to Figure 6 in S07, the projected orbital speed at this distance is 130 km s^{-1} in the north-east and 160 km s^{-1} in the south-west, making the average speed 145 km s^{-1} . We assume a value of 150 km s^{-1} as in S07. For a 40° inclination, the deprojected orbital speed is 230 km s^{-1} . Then the orbital time at 900 pc radius is 24 Myr. The pattern speed, according to L96, is $18 \text{ km s}^{-1} \text{ kpc}^{-1}$, so at the distance to the clusters, the circular speed of the pattern is 16 km s^{-1} . Thus the orbital speed relative to the pattern at the radius of the clusters is $230 - 16 = 214 \text{ km s}^{-1}$, and the orbital time relative to the pattern is $2\pi \times 900 \text{ pc} / 214 \text{ km s}^{-1} = 26 \text{ Myr}$ at 900 pc.

This relative orbital speed of 214 km s^{-1} can be multiplied by the 7 Myr age of the clusters to get the total distance they would have moved in circular orbits relative to the bar pattern. The result is 1500 pc, which corresponds to an angular displacement of $17''$ at the distance to NGC 1365, and to an arc around the center, for a circular orbit, equal to 1.7 radians or 95° . This means that if the clusters were moving in circular rotation around the center, then they would have been born somewhere near the minor axis of the bar, which is currently in the south-east – they could not have formed in their current dustlane. This possibility seems unacceptable because of their clear proximity to the northern dustlane, which is one of the few places where they could have formed, and because of the CO cloud at the position of cluster M4. It is unlikely that this cloud stayed inside the northern dustlane with the bar pattern speed and that the M4 cluster moved in a circular orbit with the orbital speed and just happened to coincide with the cloud today. More likely, both the clusters and the gas have not been moving in circular orbits.

We recently obtained SINFONI 2-D spectra for the three clusters. The analysis of these data is in progress, and they will be fully presented in a forthcoming paper (Galliano et al. in preparation). The spectra show that the radial velocity in CO and $\text{Br}\gamma$ are equal: the CO clouds are comoving with the clusters and they are all likely to be part of the inward streaming dustlane flow.

The velocity field shown in Figure 12 of S07 indicates an inward streaming speed along the bar dustlane of $\sim 40 \text{ km s}^{-1}$ in the projected image at the position of M4. Similar streaming motions are also observed in the velocity fields of optical emission lines (Lindblad et al. 1996). To get the in-plane physical speed, this 40 km s^{-1} should be corrected upward by the factor $1/(\sin \alpha \sin i) \sim 2$, where $\alpha \sim 50^\circ$ is the pitch angle of the dustlane and $i \sim 40^\circ$ is the galaxy inclination. Thus the true speed of the inflow is more like 80 km s^{-1} along the dustlane. This implies that in the last 7 Myr, the gas in the dustlane near M4 traveled inward for $\sim 560 \text{ pc}$ while it rotated around at the pattern speed for $\sim 110 \text{ pc}$. The inward distance corresponds to an angular displacement of $6.2''$ at the distance of NGC 1365. In fact, the dustlane is still dense at a position $6''$ further out from M4, so this is the likely formation site for M4 and the $5.4 \times 10^7 M_\odot$ cloud associated with it. The same could be true for the other clusters, i.e., they all formed in the north-eastern bar dustlane some 500-600 pc further out from their current position at a galactocentric distance of $\sim 1500 \text{ pc}$ ($17''$ from the center).

The suggested formation position for the clusters is highlighted in the insert in Figure 1. It is located inside the formal ILR radius given by L96, which is indicated by an ellipse, and outside the dust ring, which is at about half the ILR radius. The overall flow of gas in this region is discussed next in order to examine possible origins for the clusters.

4. Gas flow pattern in the bar and spirals

Figure 1 shows dense gas streams or filaments intersecting the bar dustlane from the interbar region. Some of these streams are traced by arrows. These dense streams have the form of arcs that can be traced back to the spiral arms on the opposite side of the galaxy. As corotation for the bar seems to be 1.31 bar lengths (L96), the brightest spiral region just outside the bar is still inside corotation. Most of the gas there should be moving inward as a result of bar and spiral torques.

The dust structure in Figure 1 suggests that the spiral arm gas does not deflect sharply at the bar end and move inward along the bar dustlane. The spiral arm dust moves from the spirals into the leading interbar region along filaments, and then it impacts the bar dustlane after curving back around at a smaller radius. Perhaps an impact like this between a small stream and the bar dustlane triggered the formation of clusters M4, M5, and M6. Each dust stream in the interbar region can be traced back through filaments to the spiral arm on the other side of the galaxy. The suggested formation site of the parent cloud for the clusters, discussed in more detail in section 8, is indicated in Figure 1. It is indeed at a place in the bar dustlane that is intersected by a filament from the interbar region.

In the south-east, the spiral arm bifurcates at about the corotation radius (Figure 1). The outer part of this bifurcation is beyond corotation for the pattern speed given by L96, so the gas and stars there should eventually move outward because of bar and spiral torques (Lynden-Bell & Kalnajs 1972; Schwarz 1981). The inner part of this bifurcation, along with the brightest parts

of the spiral arms, are inside corotation and they should eventually move inward to join the bar dustlane and ILR ring. Considering the in-streaming speed of $\sim 80 \text{ km s}^{-1}$ along the bar dustlane (see above), and the deprojected bar radius of $120''$ or 10.8 kpc for our assumed distance (JM95, L96), the time for the gas in the bar dustlane to fall in from the spiral position to the ILR is $\sim 130 \text{ Myr}$, which is 2.4 pattern rotation times (using $\Omega_p = 18 \text{ km s}^{-1} \text{ kpc}^{-1}$ from L96).

The gas flow model proposed here and based on the distribution of dust filaments in Figure 1 differs from the simulations in L96 in two important ways. First, their modeled gas flow in the bar region (their Figure 26b) has gas in one bar dustlane flow down along the dustlane and then out in the prograde direction to the other dustlane, where it shocks and gets compressed again. Then it flows out of the other dustlane in the prograde direction and back to the first dustlane. In this way, the gas circulates to the center slowly, taking 3 or more rotations relative to the bar to decrease its radius by a factor of 2 (in their Figure 26b; see also Athanassoula 1992). As a result, the net accretion rate of the dustlane gas can be small. Alternatively, the gas in the bar dustlane can go directly to the inner kpc region without emerging on the prograde side of the bar and hitting the other dustlane (e.g., Piner, Stone & Teuben 1995; Regan, Sheth, & Vogel 1999).

The primary reason for forward gas emergence out of the dustlane in some bar flow models is the assumption of an isothermal or other simplified gas equation of state. When gas is isothermal, for example, the pressure in the dustlane is large, proportional to the density, and the leading edge of the bar dustlane has a pressure gradient that accelerates the gas ahead of the lane. However, the assumption of an isothermal or other simplified gas is inappropriate for this situation. An isothermal gas has the property that every decompression has a source of energy to keep the temperature constant, but in fact there is no such source for a bar dustlane. The gas enters the dustlane, cools rapidly by CO and other molecular emission, and stays cold. There should be no significant pressure gradient at the front edge, and there should be no source of energy that would allow this gas to accelerate significantly away from the dustlane in the forward direction. The gas should fall to the central region along the bar dustlane and speed up as it moves in. Note that once the gas is in the dustlane and streaming inward, its angular momentum is already as low as it has to be to reach the inner dust ring by direct collapse. Further accretion to the nucleus depends on details of the bar potential and whether there is a nuclear bar (e.g., Knapen et al. 2002; Regan & Teuben 2004).

The assumption of an isothermal gas is useful for studies dominated by gas compression, because energy loss during compression can keep the temperature or velocity dispersion in the gas about constant. However, this assumption is inappropriate for decompression, because there is no inverse process of energy absorption to keep the velocity dispersion constant during the decompression. Interstellar shocks are a one-way path toward high density, especially if the magnetic field diffuses out rapidly in the compressed phase. The dense regions can only be broken into pieces by other shocks or clouds and only slowly evaporated to a lower density by ionization and thermal heating.

The second difference between our model and the simulations in L96 is that the spiral arm gas in L96 moves from one spiral arm to the next, losing only a small amount of orbital energy with each cycle. In Figure 1, however, one sees dense dust filaments almost radially aligned that connect the spiral arms with the bar dustlane, suggesting a gas flow directly from the spiral region to the bar, in just one-half of an orbit (in the pattern frame). A few examples of this type of flow are in Regan & Teuben (2004) for their thick bar cases (their Fig. 5).

Spiral arm streaming motions can be seen in the HI velocity map presented by JM95 (their Figures 9 and 17). Their Fig. 17 is reproduced in color here in Figure 2 because the on-line version of that paper (NASA Astrophysics Data System Bibliographic Services) has a Black and White image. On the northwest minor axis, there is a transition from positive line-of-sight velocities (red) inside corotation to negative velocities (blue) outside corotation in the same spiral arm. Because this is the near side of the galaxy, the positive velocities inside corotation are inward. On the southeast minor axis, the spiral arm velocities just inside corotation are negative (blue), which is also inward on this far side position. JM95 also note a spiral arm inflow near the bar end. From Figures 17 and 21 in JM95 (Fig. 2 here), the line-of-sight inflow speed is determined to be about -15 km s^{-1} on the near and far-side minor axes. Because these are the minor axes, the component of the inflow speed in the direction of the galactic center is $15/\sin i = 23 \text{ km s}^{-1}$ for an inclination of $i = 40^\circ$. The full flow speed along the spiral arm is this 23 km s^{-1} radial component divided by the sine of the deprojected pitch angle of the arm, which we estimate to be $\sim 25^\circ$ from the deprojected image of NGC 1365 in JM95. The full, parallel-to-arm streaming speed is thus $\sim 50 \text{ km s}^{-1}$.

In summary, the gas in NGC 1365 is observed to stream outward outside of corotation and inward inside of corotation, as expected from numerous models and observations of other galaxies. In the spiral region, the gas is mostly HI and it streams along the arms inside of corotation at a radial speed of $\sim 23 \text{ km s}^{-1}$. Some of this inflow apparently feeds dust filaments that impact and add to the bar dust lane after circling halfway around the bar pattern. The bar inflow speed is $\sim 80 \text{ km s}^{-1}$. Gas inflow should be faster and more direct than simulations suggest if the equation of state for gas does not artificially inject energy at rarefaction fronts.

5. Gas Accretion Rates, Star Formation Rates, and the Age of the Bar

There is a large reservoir of atomic gas outside the bar in NGC 1365, mostly in the spiral arms. According to Figure 4 in JM95, the projected HI column density in the northern spiral arm between the bar-end and corotation averages $\sim 13 M_\odot \text{ pc}^{-2}$. The width of the arm is $\sim 20''$ or 1.8 kpc, and the length is $\sim 200''$, or 18 kpc, so the projected area is $3.3 \times 10^7 \text{ pc}^2$. The HI mass in this part of the spiral is therefore $\sim 4 \times 10^8 M_\odot$ (independent of projection effects). The inner part of the spiral at the south-western end of the bar has a similar HI mass. Thus the total HI mass available for accretion inside corotation is $\sim 8 \times 10^8 M_\odot$ from the spiral arms alone and more from the inter-arm regions.

The radial distance the spiral arm gas has to go before reaching the bar is the spiral arm length between corotation and the bar, or ~ 3.3 kpc, considering a bar radius of 10.8 kpc and a corotation radius of 1.31 bar lengths (L96). If the radial inward speed is ~ 23 km s $^{-1}$ along the arms, as determined in the previous section, then the inflow time to the bar is the ratio of the radial distance to the radial speed, or 140 Myr. The accretion rate into the bar region from the spirals is the ratio of the accreting HI mass to the accretion time, or $\sim 5.7 M_{\odot}$ yr $^{-1}$. There could be more accretion if the gas between the spiral arms moved inward, or less if it moved outward, but these flows are unobserved.

The accretion rate along the bar dustlane can be determined in a similar way using CO data in S07. The molecular mass column density in the north-eastern dustlane increases from $\sim 40 M_{\odot}$ pc $^{-2}$ at large radius to $\sim 600 M_{\odot}$ pc $^{-2}$ in the vicinity of the clusters M4, M5, and M6. These are projected column densities, and they should be decreased by the factor $\cos 40^{\circ}$ to get perpendicular surface densities. The increase in column density with decreasing distance along the bar dustlane is consistent with the addition of gas along the dustlane from the interbar filaments, as discussed in section 4. The outermost part of the bar dustlane gets its gas partly from the local spiral and interbar region, and partly from the corotation region of the spiral arm on the other side of the galaxy, while the inner part of the bar dustlane gets its gas from the inner region of the other-side spiral arm plus the inflow along the dust lane.

The radial inflow speed at small radius, near the three clusters, is ~ 80 km s $^{-1}$, as discussed in section 3. The projected width of the bar dustlane near the clusters is 5" (see Figure 2 in G08), which is 450 pc in the direction of the minor axis. The inflow rate near the clusters is approximately the product of the projected mass column density, the projected width, and the radial inflow speed, which gives $\sim 22 M_{\odot}$ yr $^{-1}$ for the north-eastern dustlane. For the same width and accretion speed in the outer part of this dustlane, the accretion rate there is only $\sim 1.5 M_{\odot}$ yr $^{-1}$ – lower because of the lower column density. More likely, the accretion rate in the outer part of the bar dustlane is even lower than this because the gas inflow speed is lower: the gas has not yet accelerated much into the potential well of the galactic center. Midway in the bar dustlane, the molecular mass column density is $\sim 200 M_{\odot}$ pc $^{-2}$, while the width and speed are still around 450 pc and 80 km s $^{-1}$, so the accretion rate is $\sim 7 M_{\odot}$ yr $^{-1}$. All of these rates should be doubled to get the total accretion rate to the center, considering the similar dustlane on the south-western side of the bar.

There is evidently a disconnection between the rate at which the spiral arms can add mass to the outer bar region ($\sim 5.7 M_{\odot}$ yr $^{-1}$) and the rate at which the inner part of the bar dustlane adds mass to the inner kpc ($\sim 44 M_{\odot}$ yr $^{-1}$). These rates differ by a factor of ~ 8 . The spiral and bar accretion rates agree with each other fairly well in the outer part of the bar (5.7 and 3.0 M_{\odot} yr $^{-1}$, respectively), but not in the inner part. The accretion either increases by the addition of mass on the way in (e.g., in the observed interbar dust filaments), or the flow is not in a steady state.

Using the star formation rate to far-IR luminosity relation of Kennicutt (1998) and considering that half of the far-IR luminosity of the galaxy is due to the starburst, the star formation rate in

the region of the ILR was estimated to be $\sim 9 M_{\odot} \text{ yr}^{-1}$ (S07). This converts to $\sim 9.7 M_{\odot} \text{ yr}^{-1}$ for our slightly larger distance. For the total central gas mass of $9.7 \times 10^8 M_{\odot}$, the gas consumption time is short, 100 Myr (S07). However, the current nuclear accretion rate is $\sim 44 M_{\odot} \text{ yr}^{-1}$, which is about four times the star formation rate. Star formation occurs along the dustlane, as we have seen for M4, M5, and M6, converting some of the gas into stars before it reaches the center. Over the next several hundred Myr, the gas accretion rate in the center will have to decrease to the feeding rate by the spiral arms, which is $\sim 5.7 M_{\odot} \text{ yr}^{-1}$.

Eventually all of the gas inside corotation will reach the center and either turn into stars or get expelled from the region by starburst pressures. This can take longer than the current gas consumption time if the bar slows down and grows in length over time. Such bar evolution is expected because of dynamical friction on the bar exerted by the disk and halo (e.g., Athanassoula 2003, and references therein). The average HI surface density outside the bar (between 100" and 300" radius) is $\Sigma \sim 7 \times 10^{20} \text{ H cm}^{-2} \sim 6.7 M_{\odot} \text{ pc}^{-2}$, according to Figure 8 in JM95. If the bar grows at a speed v , in km s^{-1} , then this gas is added to the bar region at the rate $2\pi R \Sigma v \sim 0.4v M_{\odot} \text{ yr}^{-1}$ for a radius comparable to the bar radius of $R \sim 10 \text{ kpc}$. In Athanassoula (2003), bars can slow their pattern speed by a factor of 2 or 3 in 10^{10} years, which means their corotation radii increase by this factor in the same time. To maintain a steady accretion rate at the end of the bar that is equal to what we derived above, $5.7 M_{\odot} \text{ yr}^{-1}$, the corotation radius would have to grow at an average rate of 14 km s^{-1} . This means it would have to increase by 50%, from 10 kpc to 15 kpc, in the next 0.3 Gyr. This is faster than the corotation growth rate in the models by Athanassoula (2003), which is more like 1 km s^{-1} for a big bar.

Interactions with other galaxies could also maintain the current accretion rate to the bar region. An interaction can drive in gas from the far outer disk along tidal arms, and it can cause the bar to grow more rapidly. Perhaps a grazing collision $\sim 1 \text{ Gyr}$ ago led to the present epoch of accretion and star formation in the center.

In summary, the nuclear region of NGC 1365 is currently accreting matter at a total rate of $\sim 44 M_{\odot} \text{ yr}^{-1}$ along two dense dustlanes. This inflow adds mass to the $9.7 \times 10^8 M_{\odot}$ of molecules that is already in the ILR region, and is enough to sustain the star formation rate of $\sim 9.7 M_{\odot} \text{ yr}^{-1}$ for considerably longer than the current ILR gas consumption time of $\sim 100 \text{ Myr}$. If we consider that the total CO mass in the bar region is $3.8 \times 10^9 M_{\odot}$, from section 2, and the inner kpc already contains $0.97 \times 10^9 M_{\odot}$, then an additional gas mass of $2.8 \times 10^9 M_{\odot}$ has yet to accrete from the bar dustlanes to the central kpc. At an accretion rate of $\sim 44 M_{\odot} \text{ yr}^{-1}$, this additional gas would take an additional $\sim 63 \text{ Myr}$ to reach the ILR region. At the current star formation rate, the consumption time for this total molecular gas would be $\sim 390 \text{ Myr}$.

The central inflow rate of $\sim 44 M_{\odot} \text{ yr}^{-1}$ has no source this large in the outer part of the bar. The source there is primarily the HI that is inside corotation, and the inflow rate there is only $\sim 5.7 M_{\odot} \text{ yr}^{-1}$. At this low inflow rate, the HI reservoir inside corotation of $\sim 8 \times 10^8 M_{\odot}$ will last 140 Myr. After this 140 Myr, the HI mass inside corotation will have been added to the

current $3.8 \times 10^9 M_\odot$ of molecules in the bar region, giving a total gas mass for star formation inside corotation equal to $4.6 \times 10^9 M_\odot$. With an ILR flow rate of $\sim 44 M_\odot \text{ yr}^{-1}$, this total comes into the center in 105 Myr. At the current star formation rate of $\sim 9.7 M_\odot \text{ yr}^{-1}$, an amount of gas equal to $1.4 \times 10^9 M_\odot$ will be converted into stars in the inflow time of the HI reservoir near corotation, 140 Myr, and there will still be $3.2 \times 10^9 M_\odot$ of gas left over in the bar and central regions. This gas can continue to form stars at the same rate for another 330 Myr. Thus the current starburst can last for $140 + 330 = 470$ Myr (or $4.6 \times 10^9 M_\odot / 9.7 M_\odot \text{ yr}^{-1} = 470$ Myr), building up an additional stellar mass in the ILR and bulge region of $4.6 \times 10^9 M_\odot$, which is the total gas mass currently inside corotation. After that, the star formation rate can only be comparable to the accretion rate in the outer part of the bar from the gradual growth of the bar length. Bar growth at a likely $\sim 1 \text{ km s}^{-1}$ will add gas mass to the corotation region and ultimately to the ILR region at a rate of $0.4 M_\odot \text{ yr}^{-1}$. This will likely be the star formation rate in the ILR region after the 470 Myr period of rapid accretion is over.

Most likely, the bar is not much older than this gas consumption time, perhaps 1-2 Gyr, because there is no long-term source of gas from outside the bar region that could have maintained the current gas supply much longer than this. The gas was presumably inside corotation when the bar formed and it has been accreting and forming stars in the ILR region ever since. Because the current accretion rate exceeds the current star formation rate in the center, the bar in NGC 1365 could still be in a youthful phase where it is cleaning out the gas that was formerly in a bar-less inner galaxy disk. The central starburst could get even stronger in the next hundred million years as the rest of the bar gas comes in.

A similar time for star formation, ~ 0.5 Gyr, was suggested for the ILR ring region of the galaxy M100 by Allard et al. (2006). The bar there could be young too (1-2 Gyr) for the same reasons as given here, i.e., a lack of gas from other reservoirs. Bar ages and star formation timescales might be longer if gas from the main disk outside of corotation can also get into the bar region. Sorai et al. (2000) suggested that viscous forces might do this. Bars without active nuclear star formation would have no such constraints on their ages.

Gas accretion and star formation rates have been estimated for several other barred galaxies. Normally they are smaller than the values for NGC 1365. Meier, Turner, & Hurt (2008) measured an accretion rate of $\sim 0.7 M_\odot \text{ yr}^{-1}$ in Maffei 2, and noted that this was higher than the ILR star formation rate by a factor of 5. This result is similar to ours, suggesting sustained star formation and further gas buildup, but it is scaled down in Maffei 2 by a factor of 10 to 100 because of the smaller ILR radius (~ 100 pc compared to ~ 1 kpc). Wong & Blitz (2000) obtained inflow speeds for NGC 4736 of several tens of km s^{-1} and an accretion rate of $\sim 2 M_\odot \text{ yr}^{-1}$, which is $\sim 10\times$ higher than the inner ring star formation rate in that galaxy. Martin & Friedli (1997) derived an accretion rate ~ 4 times higher than the star formation rate in NGC 7479, which was one of the first galaxies to have an estimated accretion rate, given by Quillen et al. (1995) as $\sim 4 M_\odot \text{ yr}^{-1}$. Regan et al. (1997) obtained an accretion rate for NGC 1530 of $\sim 1 M_\odot \text{ yr}^{-1}$. Evidently, the barred galaxy studied here, NGC 1365, is unusually large and gas-rich, having a very high column

density of molecules in the inner star-forming region and a high total gas mass inside corotation. Still, it is difficult to see how it could have sustained its current level of activity for a Hubble time, given the available gas and the current rate of star formation.

We conclude that gas accretion and star formation in the ILR region of NGC 1365 is most likely variable by a factor of ~ 3 or more, as gated by the release of gas near corotation for accretion into the center, and that the total duration of the current burst might be only ~ 0.5 Gyr. The bar itself is probably not much older. Bar accretion is apparently along the bar dustlane and also along filamentary flows that leave the spiral arm region inside corotation and loop into the bar dustlane where they get assimilated. The dustlane presumably accumulates matter in this way all along its straight path to the ILR. Star formation may be triggered at the intersection points between the dustlane and the looping filaments, and it may also be triggered by spontaneous gravitational instabilities in the dustlane (section 8). Because of high pressures in the intersection points, dense massive clusters can form.

6. On the Cluster Mass Function

One peculiarity of the clusters is their large mass, $\sim 10^7 M_\odot$. Usually when clusters of this mass are found, the total mass in all clusters formed at about the same time is ~ 15 times larger for a typical cluster mass function $dN/dM \propto M^{-2}$. That is, the total mass of clusters between a minimum mass M_n and a maximum mass $M_x \sim 10^7 M_\odot$ is $M_x \ln(M_x/M_n) \sim 15M_x$ for $M_n \sim 10 M_\odot$. This implies that the total mass of clusters with comparable age in the same region should be $\sim 1.5 \times 10^8 M_\odot$, or perhaps three times larger considering there are three visible clusters each with a mass around $10^7 M_\odot$. Recall that the total gas mass inside the entire 1 kpc radius of the galaxy is $9.7 \times 10^8 M_\odot$, so the total cluster mass, considering the factor of 3, would be half of the total current gas mass. The gas mass in the region immediately surrounding the three massive clusters is $\sim 10^8 M_\odot$ from the CO(1-0) contours in Figure 2 of S07 (Sect. 2 here). This is such a small gas mass that essentially all of the other clusters that should be there in a normal cluster mass function would have had to form with nearly 100% efficiency. Moreover, these clusters would have to be obscured by dust because only the three $10^7 M_\odot$ clusters are prominent. Such obscuration is not inconceivable because the visual extinction corresponding to the average H_2 column density around the clusters, $\sim 500 M_\odot \text{ pc}^{-2}$ (S07) is ~ 35 mag – large enough to hide lower luminosity clusters. Thus we attempt to determine if there is a complement of clusters at, for example, one-tenth the mass of the observed three clusters, in the same dense dust lane with about the same age. According to the cluster mass function, there should be ten times as many clusters with one-tenth the mass of M4, M5, and M6.

We searched for these 30 expected clusters in infrared images. The region is shown in Figure 3 at three different wavelengths: on the top, from left to right are displayed the R, Ks, and [NeII] $12.8 \mu\text{m}$ narrow filter images (from G08). The dustlane region where we should search such a population of fainter clusters is indicated by a red boundary. In the visible image (R), only a few

sources are detected in this region. Because the extinction can be very large at this wavelength, this image is not well suited for looking for the fainter clusters.

In the K-band, the extinction is much lower. Inside the region of interest we can see faint sources between the three massive clusters. Measuring the fluxes of these sources is challenging because of crowding. In order to estimate how detectable a cluster is in this image, we have added an artificial source of known flux. On the bottom row of Figure 3 are shown three versions of the zoomed M4, M5, M6 region of the Ks image. This zoomed region is delineated with a white rectangle on the top middle (Ks) image. On the bottom row: to the left, the “raw” image is displayed without any added sources, in the middle, an artificial source with the same flux as M6 has been added (within the black circle), and to the right, an artificial source with 1/10th the flux of M6 has been added (within the black circle). We see that, in the latter case, the added source is at the limit of detection. However, in the original K-band image, there appear to be several tens of similar faint sources in the area of the dense dustlane. Thus, these faint sources may represent the $\sim 10^6 M_{\odot}$ part of the same cluster mass function that formed M4, M5, and M6.

If these fainter clusters had the same emission line intensities as M4, M5, or M6, then we should detect their $P\alpha$ and $Br\gamma$ line emission along the long slit $2\mu\text{m}$ spectra presented in G08. In fact, we do not detect this line emission. The lack of detection suggests that the fainter clusters have spectra with proportionally fainter nebular line emission. This observation is also consistent with the narrow band $[\text{NeII}] 12.8\mu\text{m}$ image (Figure 3, top row, right map), in which no population of faint sources can be seen. On this map, the fluxes of the three massive clusters are in the range 100 to 300 mJy, and the detection limit is down to 10 mJy. This means that there are no other $[\text{NeII}]$ emitting clusters in this region down to at least $10^6 M_{\odot}$, if the line emission is proportional to the continuum.

In summary, the dustlane region contains several tens of sources that have K-band fluxes of about 1/10th that of the most massive clusters. If these clusters formed at the same time as the massive clusters, then the initial cluster mass function could be normal, The fainter clusters do not exhibit emission line fluxes quite in proportion to their infrared luminosities, however. If they are young, then their lack of $[\text{NeII}]$ lines suggests that they removed most of their residual gas, unlike the more massive clusters which still have prominent $[\text{NeII}]$ emission. We consider possible reasons for this difference in the next section.

Alternatively, the fainter clusters could be older than the massive clusters, perhaps from earlier star formation in the ILR region. Old clusters have been found alongside young clusters in the ILR region of M100 (Allard et al. 2006). If they are indeed older, then these clusters must also be extremely massive because of their fading with age. For ages between 15 and 40 Myr, the faint clusters would be about as massive as the three younger ones (from Leitherer et al. 1999). Then the northern dust lane would contain $\sim 30 \times 10^7 M_{\odot}$ of clusters. In 40 Myr, the star formation rate required is $7.5 M_{\odot} \text{ yr}^{-1}$, which is close to the observed rate of $\sim 9.7 M_{\odot}$ (S07). In this case, there would be no obvious population of low mass clusters to make a power-law initial cluster mass

function.

7. Gas Removal from Clusters

The presence of [NeII] line emission from the most massive clusters in the inner region of NGC 1365 and the lack of any obvious emission from fainter clusters nearby could be the result of detection limitations for the fainter clusters. If, however, the low-mass clusters really do have significantly less ionized gas than the massive clusters, even less than the expected proportion to their luminosity, then this observation is somewhat peculiar. Usually, massive clusters are expected to have higher pressures for clearing away their natal gas, and so less ionized gas in proportion to their mass than lower mass clusters. Clearing depends also on gravitational self-binding of the gas, however, and it could be that lower-mass clusters have more weakly bound gas for their pressures than massive clusters.

Here we compare the energy released by a cluster’s stellar winds and supernovae to the binding energy of the residual star-forming gas. The energy released by the stars increases proportionally to the cluster mass, while the gravitational binding energy of the gas in the cluster increases like the square of the cluster mass for a fixed efficiency. Therefore, low-mass clusters should be able to clear away their gas more effectively than high-mass clusters. At some critical minimum mass, a cluster should have great difficulty removing its gas (Murray 2009). A similar mass dependence for gas expulsion that causes cluster disruption was considered by Baumgardt, Kroupa & Parmentier (2008). The tendency for high mass clusters to accrete gas from their environments was discussed by Pflamm-Altenburg & Kroupa (2009).

For the energy released by a star cluster, we consider stellar winds and supernovae with an efficiency for gas removing of 10% (MacLow & McCray 1988). For the ability of gas clearing by ionizing radiation, we consider a smaller efficiency of 0.1% (Dale et al. 2005). The time dependencies of the cluster energy outputs are computed from Starburst99 (Leitherer et al. 1999).

The energy necessary to expel gas from a cluster is approximately the binding energy,

$$E_{\text{grav}} = \frac{GM_{\text{gas}}^2}{2R} + \frac{GM_{\text{star}}M_{\text{gas}}}{R}. \quad (3)$$

The factor of 2 in the denominator of the first term in the equation comes from the reduction in the potential as the gas particles are removed.

Figure 4 plots the time dependence of the total cluster energy released multiplied by the efficiencies given above (up to 20 Myr). The gravitational binding energy, E_{grav} , is indicated by the shaded region. Three cluster masses are considered from left to right, $M_{\text{star}} = 10^5$, 10^6 , and $10^7 M_{\odot}$. The star formation efficiency is taken to be 30%. For the gas distribution radius, we take two values: (1) $R=5$ pc, in which case we consider that the gas is contained inside the radius of the stellar cluster, as derived from the HST image (G08); (2) $R=40$ pc, where we consider that the

gas bound to the cluster can have a more extended distribution. The gravitational binding energy, E_{grav} , is indicated in purple using shading for $R=40$ pc and a thick dashed purple line for $R=5$ pc. The dashed lines show the total energy values and the solid lines are the energies multiplied by the efficiencies (0.1 for mechanical energy and 0.001 for ionization energy). The total cluster energy released is the black dashed line.

Figure 4 suggests that at a cluster mass of $\sim 10^7 M_{\odot}$, the binding energy is larger than the total clearing energy available from the cluster up to ~ 7 Myr, whereas the lower mass clusters are cleared of gas more quickly. The critical mass mentioned earlier would then be $\sim 10^7 M_{\odot}$. This could explain why the three most massive clusters have not expelled their surrounding gas yet, causing them to exhibit intense [NeII] line emission. In contrast, the $\sim 10^6 M_{\odot}$ mass clusters in NGC 1365 might have been able to clear their surrounding gas in their short lifetimes, and for this reason do not show detectable [NeII] line emission.

8. Cluster Formation

The characteristic mass and separation of the largest regions of star formation in a gas disk should be comparable to the Jeans mass and Jeans length. These scales come from the dispersion relation for gravitational instabilities in a thin galaxy disk, $\omega^2 = k^2\sigma^2 - 2\pi G\Sigma k + \omega_{ep}^2$ for rate ω , wavenumber k and epicyclic frequency ω_{ep} . The wavenumber of fastest growth is $k_J = \pi G\Sigma/\sigma^2$, half the wavelength is $\lambda_J/2 = \pi/k_J = \sigma^2/G\Sigma$, and the characteristic mass is approximately the square of this half-wavelength times the column density, $M_J = \sigma^4/G^2\Sigma$. For the velocity dispersion $\sigma \sim 30$ km s $^{-1}$ of the CO gas in the region around the clusters M4, M5, and M6 (S07; Table 5), and for the average gas mass column density in the large plateau of CO gas in this region, which is $\Sigma \sim 500 M_{\odot}$ pc $^{-2}$, the Jeans mass is $M_J \sim 9 \times 10^7 M_{\odot}$. This is not much different from the cloud mass in the immediate neighborhood of M4, which is $5.4 \times 10^7 M_{\odot}$ (for our distance assumption).

Similarly, the wavelength of the instability is $\lambda_J = 830$ pc. The observed separation between M4 and M5 is 4" parallel to the major axis, which is 360 pc at the distance of 18.6 Mpc. Between M5 and M6 the projected distance is also 4", but these clusters are oriented in the direction of the minor axis. Correcting for an inclination of 40°, their separation becomes 470 pc. These cluster separations are about half the current Jeans length.

The cluster separations at the time of their formation, 7 Myr ago, would have been larger if the clusters have each fallen toward the center of the large CO plateau in which they are currently located, which means fallen toward each other. The acceleration rate toward the center of the plateau is $A = G\Sigma$ for $\Sigma \sim 500 M_{\odot}$, and the distance they would have moved in $t = 7$ Myr is $0.5At^2 = 55$ pc. Thus their separations could have been larger by ~ 110 pc when they formed if they each fell toward their common center by 55 pc. This 110 pc, when added to the current separation of ~ 400 pc, is 60% of λ_J . Considering the uncertainties with σ , Σ , the dispersion relation, and the physical interpretation of λ_J for a complex environment, the overall scale of clustering in this

region is basically consistent with a model in which star formation is driven by gaseous self-gravity. This conclusion is consistent with the agreement between the total nuclear star formation rate and the expectations from the Kennicutt (1998) relation, given the molecular surface density in the region (S07).

For the average plateau molecular density of 95 cm^{-3} derived in Section 2, the dynamical time for cloud formation is $(G\rho)^{-1/2} \sim 6.3 \text{ Myr}$. If the cloud-forming plateau moved inward along the bar dustlane at the same speed as the rest of the gas, 80 km s^{-1} , then the formation of the parent clouds that made the clusters began $\sim 13 \text{ Myr}$ ago, 6.3 Myr before the birth of the clusters, at a distance from the current clusters of $\sim 1.0 \text{ kpc}$. This is $11''$ (deprojected) further out from the current cluster positions along the bar dustlane.

Figure 1 indicates the approximate cloud formation position. It is at a place in the dustlane where there is currently an intersection with a filament extending to the interbar region. Such filaments would have a timescale for changes comparable to the timescale for the gas flow from the spiral region to the bar dust lane. For a pattern speed of $18 \text{ km s}^{-1} \text{ kpc}^{-1}$ and an orbit speed of 230 km s^{-1} at a mean galactocentric radius of $\sim 3 \text{ kpc}$ (section 3) the half-orbit time relative to the bar pattern is $\pi (230 \text{ km s}^{-1}/3 \text{ kpc} - 18 \text{ km s}^{-1}/\text{kpc})^{-1} = 50 \text{ Myr}$. This is slightly larger than the timescales for cloud and cluster formation given above. It seems plausible that massive cluster formation was triggered in the densest part of the bar dustlane by the impact of a stream of gas flowing from the spiral arm region on the other side of the galaxy. This is similar to the scenario proposed by Böker et al. (2008) in which cluster formation takes place at the intersection point between the straight bar dust lane and the circular ILR ring. In our case, the trigger in the bar dust lane would be the gas falling into the bar from large radii on the other side. Our model is closer to that of Sheth et al. (2000), who noted the presence of dust spurs on the trailing sides of the bar dust lane in NGC 5383 at approximately the same positions as HII regions on the leading side. They suggested that stars formed in the spurs and then pushed through the dust lane to emerge at the leading side. Asif et al. (2005) made a similar suggestion for NGC 4151 based on the velocities of HII regions associated with star formation near the bar dustlane. Zurita & Pérez (2008) thought that this process operated in NGC 1530 based on an age gradient in HII regions perpendicular to the bar, and they also found the motion of spur gas toward the dust lanes. The filaments discussed in the present paper are apparently the same as the spurs in NGC 5383 and NGC 1530. We suggest that star formation may not occur in the spurs or filaments themselves, but in the intersection points between these gas streams and the dust lane as a result of local dust lane compression and triggered instabilities. The emergence of stars or clusters out the front of the dust lane, if this happens, could then be the result of the initial stream momentum transferred to the compressed gas.

Massive dense clusters require very high gas pressures to form. The total kinematic pressure from stellar motion in the cluster today is $\sim 0.1GM_{\text{star}}^2/R^4 \sim 10^{11}k_B$ for $M_{\text{star}} \sim 10^7 M_{\odot}$ and $R \sim 5 \text{ pc}$ core radius, and 10^8k_B for $R \sim 40 \text{ pc}$ overall. These are 10 to 10^4 times the average disk gas pressure discussed in section 2. We suggested above that the inflowing filaments impact the

bar dustlane and make the dustlane pressure high. This is the usual explanation for a dustlane: it is a shock front in either a spiral arm or a bar caused by the sudden deflection and compression of incoming gas. The point here is that the incoming gas is apparently visible in the form of interbar dust filaments. Because such filaments touch the bar dustlane in a few discrete points, the pressures should be unusually high there, possibly triggering star formation. If we consider that the density in a filament is ~ 0.1 times that of the dustlane, or $5 \text{ H}_2 \text{ cm}^{-3}$, based on the lower extinction in the filaments shown in Figure 1, and that their impact speed is the relative speed between a circular orbit and the bar at this radius, 214 km s^{-1} as given in section 3, then the impact ram pressure of the filament on the dustlane is $7 \times 10^7 k_B$. This is about right to generate the dustlane pressure and the pressure in the cluster-forming cloud. The higher pressure in the cluster core is presumably the result of self-gravitational contraction in the molecular cloud.

9. Conclusions

The three massive clusters in the center of NGC 1365, along with a large number of other fainter clusters in the same region, apparently formed ~ 7 Myr ago in a giant molecular cloud, the remnants of which are still visible today (S07). This cloud formed another ~ 6 Myr earlier in the inner part of the bar dustlane. The cloud and the clusters are flowing inward at $\sim 80 \text{ km s}^{-1}$ and should soon join the dust ring inside the ILR as they arc around on the far side of the nucleus. It is conceivable that subsequent events of star formation like this will produce a regular sequence of cluster ages around the inner ring, as observed in M100 by Ryder, Knapen & Takamiya (2001) and Allard et al. (2006), and in several other galaxies by Böker et al. (2008) and Mazzuca et al. (2008). The formation mechanism of the clusters is probably a gravitational instability in the molecular cloud, which itself probably formed by self-gravitational gas dynamics in the moving dustlane, perhaps triggered by the impact of an interbar filament that is observed at the likely location of cloud formation.

Gas moves in the bar region partly through arching filaments that come from spiral arms inside corotation, and partly through straight bar dustlanes, where the gas plunges into the ILR ring. The accretion rate from the spirals and the outer parts of the bar dustlanes is $\sim 5.7 M_\odot \text{ yr}^{-1}$, while the accretion rate in the inner parts of the bar dustlanes is $\sim 44 M_\odot \text{ yr}^{-1}$. The inner accretion rate, combined with the current gas reservoir, can sustain the nuclear star formation rate for ~ 0.5 Gyr. The bar itself is probably not much older than this, considering the lack of any source of gas to replenish the accretion.

Starbursts in the ILR regions of barred galaxies can be driven by rapid accretion of gas inside corotation as it flows from the spiral region through the interbar region to the bar and then down the bar dustlanes. Simulations that suggest a more gradual spiraling of gas to the center use an equation of state that artificially introduces thermal energy at rarefaction fronts, providing a source of pressure that is not likely to be present in a real galaxy. Massive clusters form because the self-gravitational pressure in the inner disk can be extremely large, close to $10^8 k_B$. The most massive

clusters may retain their gas longer than lower-mass clusters because of their higher gravitational binding energy per unit cluster luminosity. These massive clusters can then dominate the ionization and emission of [NeII], giving the impression that they form alone. In fact, there are probably lower-mass clusters present too, in the usual proportion.

10. Acknowledgements

We are gratefully indebted to F. Bournaud for interesting discussions and to the referee for useful comments. BGE is grateful to CEA/Saclay for support during a June 2008 visit when this work began. DA thanks CEA/Saclay for supporting a March 2009 trip to the Rio observatory, when this work was finalized.

REFERENCES

- Allard, E. L., Knapen, J. H., Peletier, R. F., Sarzi, M. 2006, MNRAS, 371, 1087
- Asif, M.W., Mundell, C.G., & Pedlar, A. 2005, MNRAS, 359, 408
- Athanassoula, E. 1992, MNRAS, 259, 345
- Athanassoula, E. 2003 MNRAS 341 1179
- Barth, A.J., Ho, L.C., Filippenko, A.V., Sargent, W.L. 1995, AJ, 110, 1009
- Baumgardt, H., Kroupa, P. & Parmentier, G. 2008, MNRAS, 384 1231
- Benedict, G.F. et al. 1993, AJ, 105, 1369
- Böker, T., Falcón-Barroso, J., Schinnerer, E., Knapen, J.H., & Ryder, S. 2008, AJ, 135, 479
- Buta, R. & Combes, F. 1996, Fundamentals of Cosmic Physics, 17, 95
- Combes, F., & Gerin, M. 1985, A&A, 150, 327
- Dale, J. E., Bonnell, I. A., Clarke, C. J., & Bate, M. R. 2005, MNRAS, 358, 291
- Elmegreen, B.G. 1994, ApJ, 425, L73
- Elmegreen, B.G. 1989, ApJ, 338, 178
- Emsellem, E., Greusard, D., Combes, F., Friedli, D., Leon, S., Pécontal, E., & Wozniak, H. 2001, A&A, 368, 52
- Fall, S. M., & Zhang, Q. 2002, IAUS, 207, 566

- Forbes, Duncan A., & Norris, R. P. 1998, MNRAS, 300, 757
- Galliano, E., Alloin, D., Pantin, E., Lagage, P. O., & Marco, O. 2005, A&A, 438, 803
- Galliano, E., Alloin, D., Pantin, E., Granato, G. L., Delva, P., Silva, L., Lagage, P. O., & Panuzzo, P. 2008, A&A, 492, 3 (G08)
- Hummel, E., van der Hulst, J. M., & Keel, W. C. 1987, A&A, 172, 32
- Ishizuki, S., Kawabe, R., Ishiguro, M., Okumura, S.K., Morita, K.-I. 1990, Nature, 344, 224
- Jogee, S., Scoville, N., & Kenney, J.D.P. 2005, ApJ, 630, 837
- Jörsäter, S., & van Moorsel, G. A. 1995, AJ, 110, 2037 (JM95)
- Kenney, J.D.P., Wilson, C.D., Scoville, N.Z., Devereux, N.A., & Young, J.S. 1992 ApJ, 395, L79
- Kennicutt, R.C., Jr. 1998, ApJ, 498, 541
- Knapen, J. H., Shlosman, I., Heller, C. H., Rand, R. J., Beckman, J. E., & Rozas, M. 2000, ApJ, 528, 219
- Knapen, J. H., Pérez-Ramrez, D., Laine, S. 2002, MNRAS, 337, 808
- Kormendy, J., & Kennicutt, R.C., Jr. 2004, ARAA, 42, 603
- Kristen, H., Jörsäter, S., Lindblad, P.O., & Boksenberg, A. 1997, A&A, 328, 483
- Leitherer, C., Schaerer, D., Goldader, J.D., et al., 1999, ApJS, 123, 3
- Lindblad, P.A.B., Lindblad, P.O., & Athanassoula, E. 1996, A&A, 313, 65 (L96)
- Lindblad, P. O., Hjelm, M., Hoegbom, J., Joersaeter, S., Lindblad, P. A. B., Santos-Lleo, M. 1996, A&AS, 120, 403
- Lynden-Bell, D. & Kalnajs, A.J. 1972, MNRAS, 157, 1
- MacLow, M-M. & McCray, R. 1988, ApJ, 324, 776
- Maoz, D., Barth, A. J., Sternberg, A., Filippenko, A. V., Ho, L. C., Macchetto, F. D., Rix, H.-W., Schneider, D. P. 1996, AJ, 111, 2248
- Maoz, D., Barth, A.J., Ho, L.C., Sternberg, A., & Filippenki, A.V. 2001, AJ, 121, 3048
- Martin, P., & Friedli, D. 1997, A&A, 326, 449
- Mazzuca, L.M., Knapen, J.H., Veilleux, S., & Regan, M.W. 2008, ApJS, 174, 337
- Meier, D.S., Turner, J.L., & Hurt, R.L. 2008, ApJ, 675, 281

- Meurer, G. R., Heckman, T. M., Leitherer, C., Kinney, A., Robert, C., & Garnett, D. R. 1995, AJ, 110, 2665
- Morgan, W.W. 1958, PASP, 70, 364
- Morganti, R., Tsvetanov, Z. I., Gallimore, J., & Allen, M. G. 1999, A&AS, 137, 457
- Murray, N., 2009, ApJ, 691, 946
- Parmentier, G., & Gilmore, G. 2005, MNRAS, 363, 326
- Pflamm-Altenburg, J., & Kroupa, P. 2009, MNRAS, 397, 488
- Piner, B. G., Stone, J. M., & Teuben, P. J. 1995, ApJ, 449, 508
- Quillen, A.C., Frogel, J.A., Kenney, J.D.P., Pogge, R.W., & DePoy, D.L. 1995, ApJ, 441, 549
- Regan, M. W., Vogel, S.N., Teuben, P.J. 1997, ApJ, 482, 135
- Regan, M.W., Sheth, K., & Vogel, S.N. 1999, ApJ, 526, 97
- Regan, M.W., Sheth, K., Teuben, P.J., & Vogel, S.N. 2002, ApJ, 574, 126
- Regan, M.W., Teuben, P. 2003, ApJ, 582, 723
- Regan, M.W., & Teuben, P.J. 2004, ApJ, 600, 595
- Ryder, S.D., Knapen, J.H., & Takamiya, M. 2001, MNRAS, 323, 663
- Sakamoto, K., Okumura, S. K., Ishizuki, S., & Scoville, N. Z. 1999, ApJ, 525, 691
- Sakamoto, K., Ho, Paul T. P., Mao, R.-Q., Matsushita, S., & Peck, A.B. 2007, ApJ, 654, 782 (S07)
- Sanders, R.H., & Huntley, J.M. 1976, ApJ, 209, 53
- Sandqvist, A., Joersaeter, S., & Lindblad, P. O. 1995, A&A, 295, 585
- Schwarz, M.P. 1981, ApJ, 247, 77
- Sersic, J.L., & Pastoriza, M. 1965, PASP, 77, 287
- Sheth, K., Regan, M.W., Vogel, S.N., & Teuben, P.J. 2000 ApJ, 532, 221
- Sheth, K., Vogel, S.N., Regan, M.W., Teuben, P.J., Harris, A.I., & Thornley, M.D. 2002, AJ, 124, 2581
- Sheth, K., Vogel, S.N., Regan, M.W., Thornley, M.D., & Teuben, P.J. 2005, ApJ, 632, 217
- Sorai, K., Nakai, N., Kuno, N., Nishiyama, K., Hasegawa, T. 2000, PASJ, 52, 785

Tacconi-Garman, L. E., Sternberg, A., & Eckart, A. 1996, *AJ*, 112, 918

Vesperini, E. 2000, *MNRAS*, 318, 841

Wong, T., & Blitz, L. 2000, *ApJ*, 540, 771

Zurita, A., Relaño, M., Beckman, J.E., & Knapen, J.H. 2004, *A&A*, 413, 73

Zurita, A., & Pérez, I. 2008, *A&A*, 485, 5

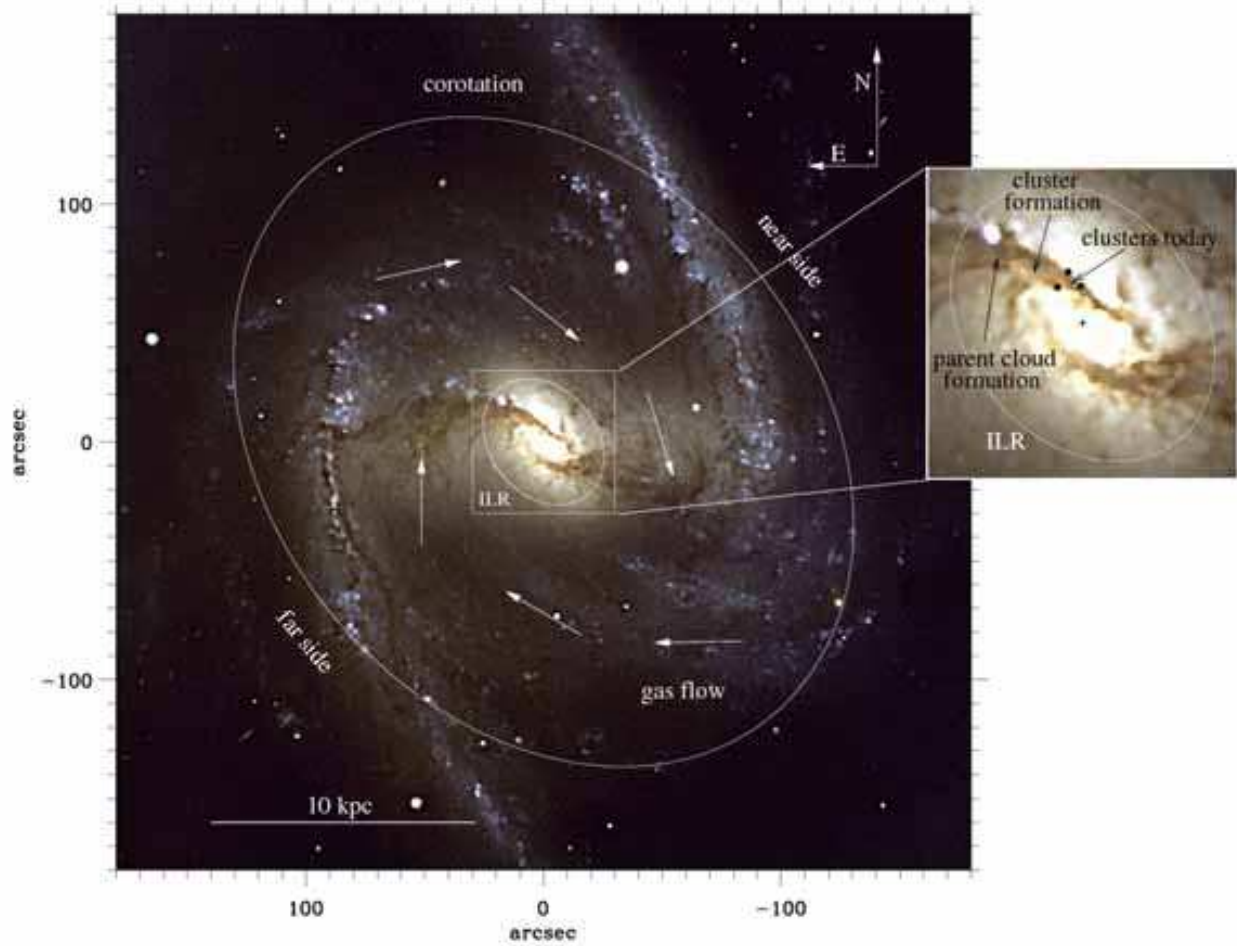


Fig. 1.— Optical image of NGC 1365 from three exposures with FORS1: B(blue), V(green), and R(Red). Overlays show the corotation radius, suggested flow lines based on dust filaments, the current positions of the clusters M4, M5, and M6, and the suggested formation positions of these clusters and their parent molecular cloud, based on ages, dynamical times, and gas velocities. (Image degraded for arXiv. see Fig1astroph.jpg)

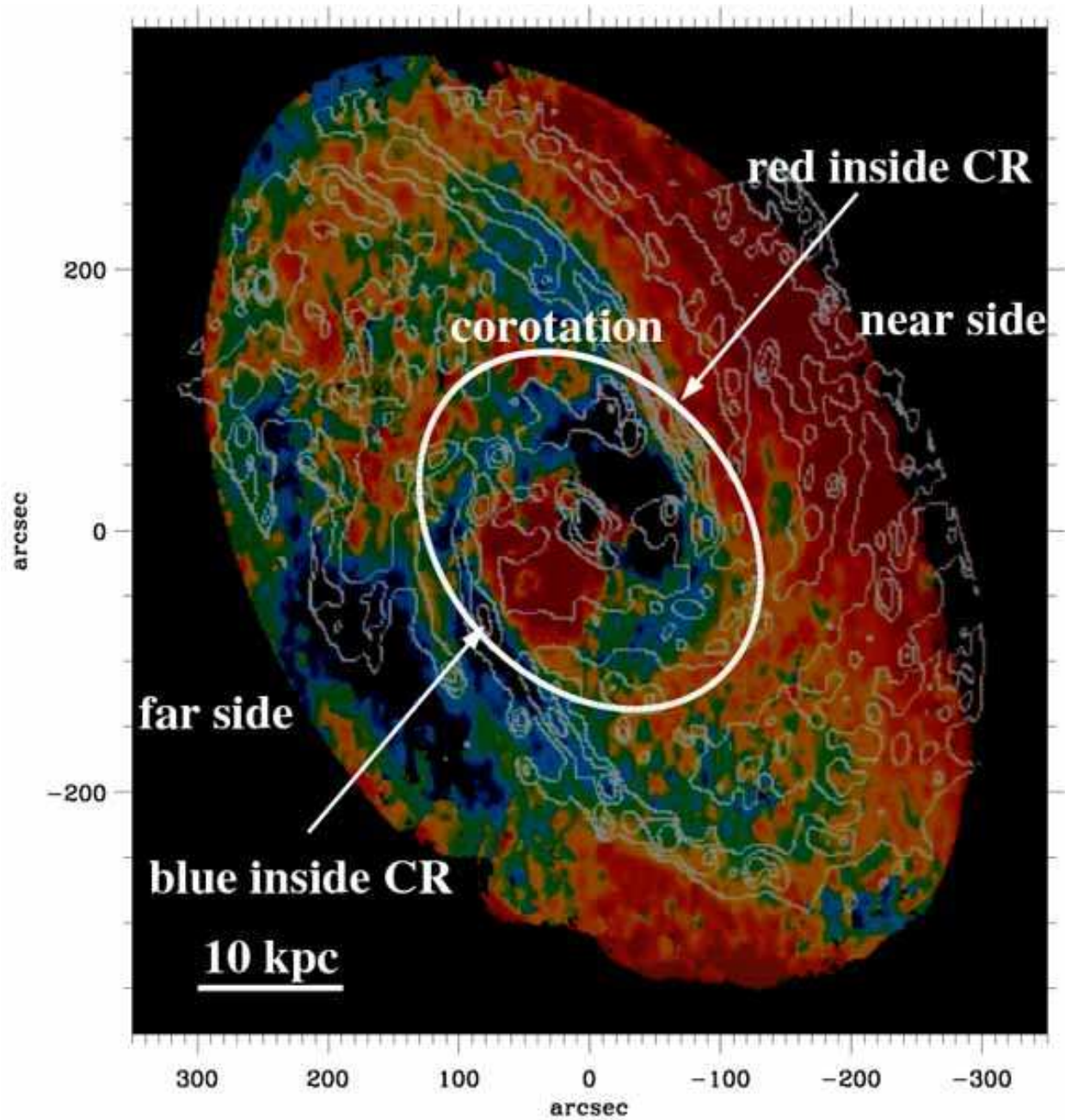


Fig. 2.— Reproduction of the HI velocities (color) and B-band optical intensities (contours) of NGC 1365 from Figure 17 of JM95, with notation added. The color scale ranges from -25 km s^{-1} in the extreme blue to $+25 \text{ km s}^{-1}$ in the extreme red. The sign of spiral arm streaming changes at corotation from inward inside corotation to outward outside corotation, as indicated by the color change. (Image degraded for arXiv. see Fig2astroph.jpg.)

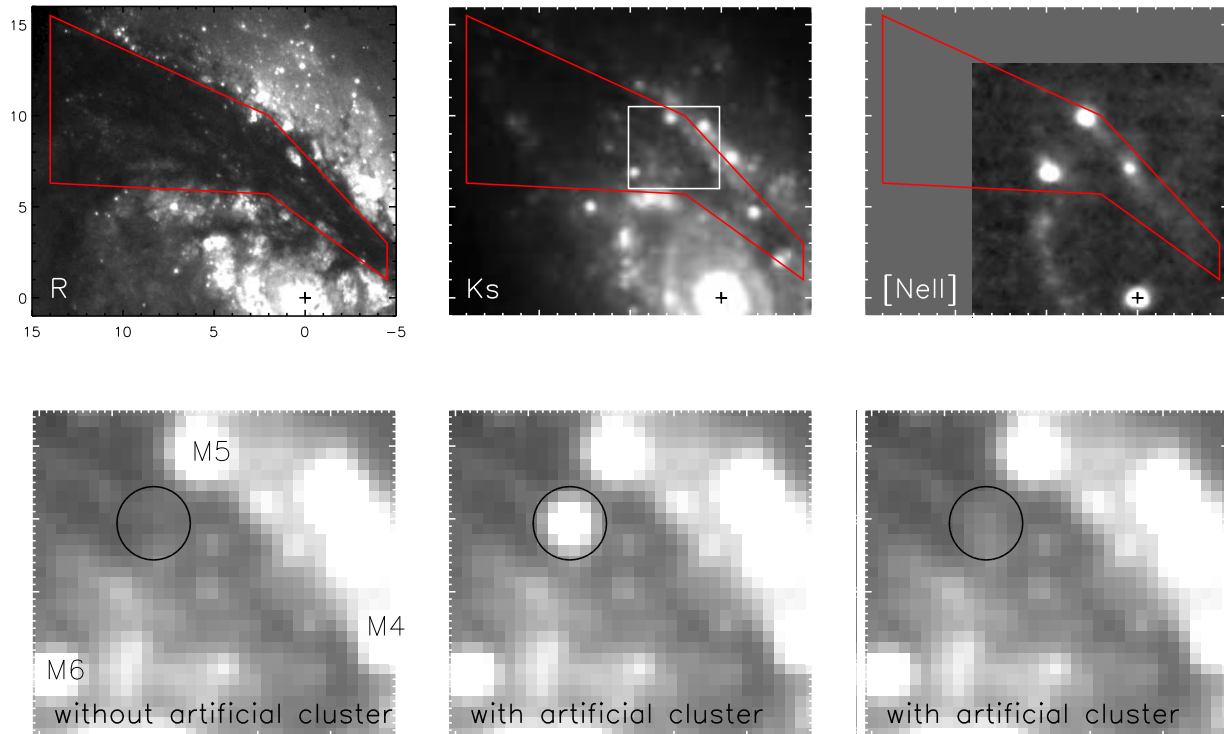


Fig. 3.— The top three panels show the inner region of NGC 1365 surrounding the bar dust lane in the north in R, Ks, and [NeII] $12.8 \mu\text{m}$ narrow filter images. The active galactic nucleus is identified with a cross. The bottom three panels show an enlargement in the Ks band of the region inside the white rectangle in the top where the three massive clusters are. The bottom left shows the raw image, the bottom center shows the same image but with the addition of an artificial source having the same flux as M6. The bottom right has an artificial source with 1/10th the flux of M6. The 1/10th artificial source is barely detectable, as are similarly faint real sources in this image. Evidently, there are several tens of clusters in this region with masses of ~ 0.1 times the mass of M6 if they all have the same age.

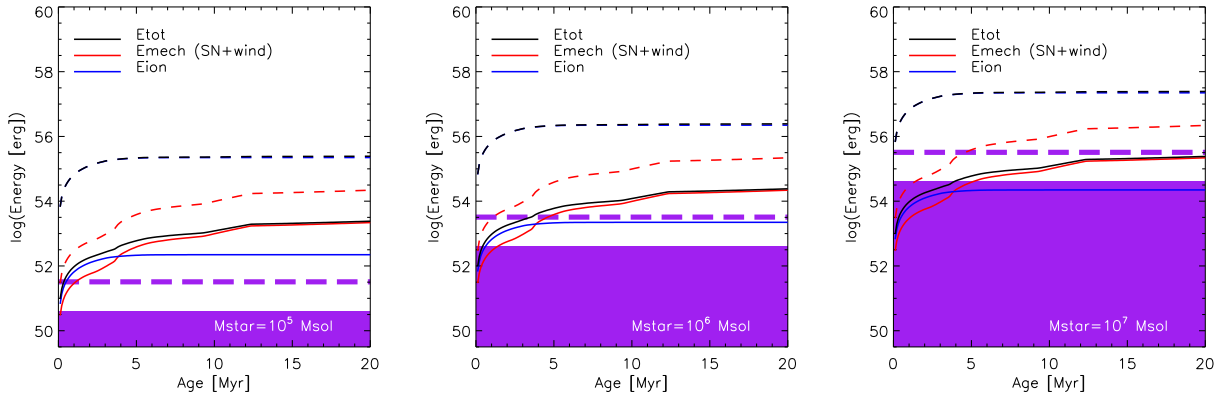


Fig. 4.— Models showing the energy sources and sinks for clusters with masses of 10^5 , 10^6 , and $10^7 M_{\odot}$, from left to right. The dashed lines are the total energies put out by the clusters in the three forms indicated: total, mechanical (supernovae and stellar winds), and ionization. The solid lines are these energies multiplied by the efficiencies for pushing cluster gas away. The gravitational binding energy is shown in purple, with shading for $R=40$ pc and a thick dashed line for $R=5$ pc. The gas mass is assumed to be 2.3 times the star mass. This figure suggests that low mass clusters put out an amount of energy that can clear the gas away within only a million years, while a $10^7 M_{\odot}$ cluster cannot clear the gas away for ~ 7 Myr. This result may explain why the three massive clusters still emit [NeII] while the low mass clusters nearby do not.

This figure "Fig1astroph.jpg" is available in "jpg" format from:

<http://arxiv.org/ps/0907.2602v2>

This figure "Fig2astroph.jpg" is available in "jpg" format from:

<http://arxiv.org/ps/0907.2602v2>